Ion heating and magnetohydrodynamic dynamo fluctuations in the reversed-field pinch

Earl Scime,[a] Miodrag Cekic, D. J. Den Hartog, Samuel Hokin, D. J. Holly, and Christopher Watts
Department of Physics, University of Wisconsin—Madison, Madison, Wisconsin 53706

(Received 8 June 1992; accepted 18 August 1992)

Ion temperatures have been measured in the Madison Symmetric Torus (MST) [Dexter *et al.*, Fusion Technol. **19**, 131 (1991)] reversed-field pinch (RFP) with a five channel charge exchange analyzer. The characteristic anomalously high ion temperature of RFP discharges has been observed in the MST. The ion heating expected from ion–electron collisions is calculated and shown to be too small to explain the measured ion temperatures. The charge exchange determined ion temperature is also compared to measurements of the thermally broadened Cv 227.1 nm line. The ion temperature, $T_i \approx 250$ eV for $I = 360$ kA, increases by more than 100% during discrete dynamo bursts in MST discharges. Magnetic field fluctuations in the range 0.5–5 MHz were also measured during the dynamo bursts. Structure in the fluctuation frequency spectrum at the ion cyclotron frequency suggests that the mechanism of ion heating involves the dissipation of dynamo fluctuations at ion cyclotron frequencies.

I. INTRODUCTION

Despite the progress in magnetic confinement fusion since the first reversed-field pinch (RFP) discharge was accidentally formed in the ZETA experiment in 1960,[1] many of the fundamental questions regarding reversed-field pinch plasmas at that time remain unanswered today. Among these questions are: What is the physical mechanism that produces and sustains the toroidal field (the dynamo effect) and why are the ions often as hot, if not hotter, than the electrons in Ohmically heated plasmas? This paper addresses the second question by presenting experimental measurements of the ion temperature in the Madison Symmetric Torus (MST).[2]

In a classical Ohmic discharge, only the electrons are directly heated, so the ions must be heated by ion–electron thermal equilibration. In many RFP's and early tokamaks, however, ion temperatures greater than electron temperatures have been observed.[3–7] Therefore, the ions must acquire energy through some channel that bypasses the bulk electron population. Other magnetic confinement devices that internally generate magnetic fields, e.g., spheromaks and field-reversed configurations, have also reported anomalously high ion temperatures.[8] Ion temperatures equal to and greater than the electron temperature have been observed in MST discharges, and it will be shown that the ion temperature exceeds what could be reasonably expected from ion–electron collision heating.

Because of the large magnetic fluctuations in the RFP,[9] on the order of a few percent, a number of researchers have proposed that somehow the energy stored in the fluctuations is transferred to the ions as the fluctuations are dissipated.[10,11] There has been considerable evidence that not all of the energy flowing into Ohmically heated RFP plasmas heats the electrons or is emitted as radiation.[10,11] The series of experiments presented in this paper were designed to investigate the correlation between measured increases in dynamo fluctuation activity and measured increases in the plasma ion temperature. These results demonstrate a clear correlation between the mechanism responsible for generating the toroidal magnetic field (the dynamo) and ion heating in the RFP. Throughout this paper, the magnetohydrodynamic (MHD) dynamo model, which relies upon correlated magnetic field and fluid velocity fluctuations to explain the dynamo effect,[12] is used to describe the mechanism responsible for the internal generation of toroidal field.

The apparatus used in these experiments is briefly reviewed (Sec. II) and then measurements of the equilibrium and nonequilibrium ion temperature are discussed (Secs. III and IV). The magnetic field fluctuation measurements which suggest that ion cyclotron resonances may be the physical mechanism responsible for the ion heating in the RFP are presented in Sec. V.

II. APPARATUS

The experiments discussed in this report were performed on the University of Wisconsin's Madison Symmetric Torus. The MST is a modern, large ($R = 1.5$ m, $a = 0.52$ m), toroidal confinement device that is typically operated in a reversed-field pinch configuration. The MST has been described in detail elsewhere[2] and only those features of the MST that have a direct bearing on the ion temperature and magnetic fluctuation measurements are reviewed here.

The shell of the MST is both the vacuum vessel and a single turn toroidal field coil.[2] This results in a very low ripple toroidal field; however, it may also be responsible for the dramatic changes in toroidal flux, hereafter called dynamo bursts, that occur throughout reversed-field pinch discharges in the MST (Fig. 1). When run as a RFP, the

[a]Present address: Los Alamos National Laboratory, Los Alamos, New Mexico 87545.

 0899-8213/92/124062-10$04.00 © 1992 American Institute of Physics

Downloaded 07 Jun 2006 to 128.104.165.52. Redistribution subject to AIP license or copyright, see http://pop.aip.org/pop/copyright.jsp

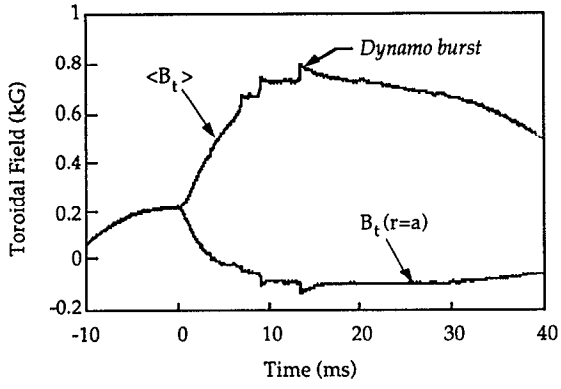

FIG. 1. Average and edge toroidal field in the MST. Discharge begins at $t=0$.

toroidal field in MST is almost entirely self-generated. Losses of toroidal flux must be replaced by the internal dynamo mechanism and the dramatic increases in toroidal flux are indicative of sharp increases in the level of dynamo activity. The nonzero resistance and inductance of the toroidal field circuit prevents the shell from responding quickly enough to act as a perfect flux conserver, which would suppress rapid toroidal flux changes. Changes in the external circuit impedance affect the level of internal dynamo activity by altering the amount of toroidal flux lost during the discharge. Other RFP's (ZT-40M,[5] Repute-1,[13] Eta-Beta II,[14] and HBTX[6]) have also reported cyclic fluctuations in reversal and pinch parameters (F and Θ), but only the oscillations reported by ZT-40M during high pinch parameter operation are similar to the distinct bursts of dynamo activity in the MST.

The principle diagnostics used for these experiments were a five channel charge exchange analyzer[15,16] and a high-frequency magnetic fluctuation probe inserted at the plasma edge.[16] Other diagnostics also used for these experiments included: a Thomson scattering diagnostic,[17] a seven-channel vacuum ultraviolet spectrometer, conventional flux and Rogowski loops, and a far-infrared laser interferometer.[18] Doppler ion temperature measurements from the ultraviolet spectrometer provided a quantitative benchmark for comparison with the charge exchange ion temperatures.

The details of the fast time resolution, 10 μsec, charge exchange analyzer constructed for these experiments are described elsewhere.[15,16] Due to space considerations, only a brief review of charge exchange analysis will be presented here. Further information can be found in many texts.[19] The isotropically emitted neutral emission rate [#/sec] of energy E in the energy interval dE collected by a detector subtending the solid angle Ω_s at the surface of a hot plasma is given by[19]

$$F(E)dE=v^2\,dv\,\Omega_s\int\exp\left(-\int_z^a\alpha(l)dl\right)S(\mathbf{x},\mathbf{v})d^3\mathbf{x},$$

where

$$\exp\left(-\int_z^a\alpha(l)dl\right)$$

is the probability that a neutral atom at position $\mathbf{x}$ in the interior travels along the detector's line of sight to the edge without undergoing an ionizing collision and

$$\alpha=(1/v)[\langle\sigma_{ei}v_e\rangle_v n_e+(\langle\sigma_{pi}v_i\rangle_v+\langle\sigma_{cx}v_i\rangle_v)n_i]$$

is the attenuation coefficient for the neutrals. Here σ_{ei}, σ_{pi}, and σ_{cx} are, respectively, the electron ionization, proton ionization, and charge exchange cross sections; $S(\mathbf{x},\mathbf{v})d\mathbf{v}$ is the total birth rate of neutrals of velocity $\mathbf{v}$ in the velocity element $d\mathbf{v}$ at a position $\mathbf{x}$.[19] Although S includes recombination, charge exchange is the dominant process at typical MST plasma densities and temperatures. Assuming that the background neutral population arises from the transport of the cold edge fueling gas into the plasma, the energy of the neutral can be ignored during the charge exchange process and the neutral emission can be written as[19]

$$F(E)dE\approx v^2\,dv\,\Omega_s[\sigma_{cx}(E)v(E)]\times\int\exp\left(-\int_z^a\alpha(l)dl\right)n_H(\mathbf{x})f_i(\mathbf{x},\mathbf{v})d^3\mathbf{x}.$$

Assuming the ion distribution f_i is a Maxwellian, the dominant contribution to neutral flux (along $\hat{x}$) measured at energies such that $E\gg T$ occurs at $T_i'=0$ (where T_i is a maximum). The non-line-of-sight spatial integration is defined by the apertures of the analyzer and the dominance of the hot part of the plasma along the line of sight can be used to approximate the line-of-sight integral:[16]

$$F(E)dE\approx\xi A\Omega_s\sigma_{cx}E\,dE\left(\frac{n_H(z^*)n_i(z^*)}{\sqrt{2m_i}[\pi T(z^*)]^{3/2}}\right)\times\exp\left(-\frac{E}{T(z^*)}\right)\exp\left(-\int_{z^*}^a\alpha(l)dl\right),$$

where z^*=point of maximum temperature along line of sight and ξ is used to approximate the width of the line-of-sight integrand (ξ has units of cm). Assuming that the attenuation of the neutral emission is negligible, this expression can be rewritten as

$$\frac{dN}{dE}=\frac{F(E)}{A\Omega_s\xi\sigma_{cx}(E)E}\approx\left(\frac{n_H(z^*)n_i(z^*)}{\sqrt{2m_i}[\pi T_i(z^*)]^{3/2}}\right)\exp\left(-\frac{E}{T_i(z^*)}\right),\qquad(1)$$

where $dN/dE=\#/(\text{sec cm}^5\text{ st eV}^2)$, F is the rate of neutral emission of energy E in energy interval dE, $A\Omega_s$ is the etendue of charge exchange analyzer with respect to the plasma, $n_H(z^*)$ is the neutral density of plasma at hottest point along line-of-sight (z^*), $n_i(z^*)$ is the ion density of plasma at hottest point along line-of-sight, and $T_i(z^*)$ is the peak ion temperature along line-of-sight.

The ion temperature can be determined from the inverse slope of a logarithmic plot of dN/dE versus energy, or from a nonlinear fit to the full expression. The neutral

Downloaded 07 Jun 2006 to 128.104.165.52. Redistribution subject to AIP license or copyright, see http://pop.aip.org/pop/copyright.jsp

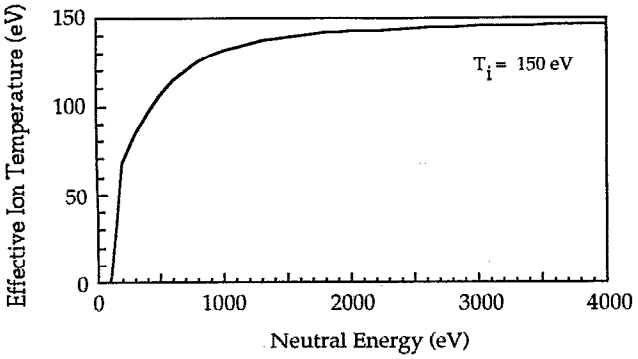

FIG. 2. Ion temperature calculated from slope of log plot of corrected flux at a particular neutral energy. Actual central ion temperature is 150 eV, so the simple calculation slightly underestimates the central ion temperature. Results are from the NEUCG neutral transport code.

transport code NEUCG,[20] which self-consistently calculates the neutral density profile, was used to generate theoretical neutral flux emission spectra for typical MST parameters. The central ion temperature that would be obtained from the slope of the neutral flux spectrum at a particular energy for a MST plasma with parabolic density and temperature profiles is displayed verses energy in Fig. 2. The true central ion temperature for the case shown in Fig. 2 is 150 eV. So at neutral sampling energies of 2000 eV, this simple temperature calculation technique underestimates the central ion temperature by 10%–20%. A typical experimental neutral energy spectrum and logarithmic fit are shown in Fig. 3.

Sampling the neutral energy spectrum at more than one energy point eliminates the need for profile assumptions in the simple temperature calculation, however, to obtain absolute neutral flux measurements, density and temperature profiles have to be assumed in order to calculate ξ. Throughout this paper, parabolic ion temperature and density profiles have been assumed for the absolute flux calculations.

For ion temperature fluctuation measurements, the possibility of profile induced changes in the calculated ion temperature is a critical issue. To affect the calculated ion

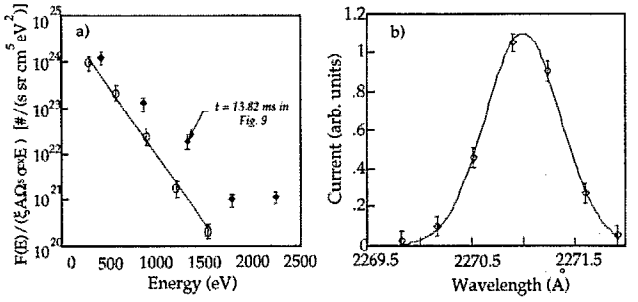

FIG. 3. Spectra used for ion temperature calculations. (a) Typical neutral energy spectrum and logarithmic fit (circles). Non-Maxwellian neutral energy spectrum just before the peak of the dynamo burst (diamonds)—see Fig. 9. (b) Typical Cv Doppler broadened spectrum for Fig. 4.

TABLE I. Typical plasma parameters for the experiments in this report.

Parameter	Value
Plasma current (kA)	350
Loop voltage (V)	15
Central electron temperature (eV)	325
Central ion temperature (eV)—CXA	300
Central electron density (cm^{-3})	$\sim 1\times 10^{13}$
Energy confinement time (msec)—estim.	$\leqslant 1.0$
Plasma duration (msec)	60

temperature by more than 20% while keeping the central ion temperature fixed requires substantial changes in the plasma density and density profile. Simulation results using the NEUCG code indicate that a change in the calculated ion temperature of 30% requires a change in the line-averaged plasma density, $\bar{n}_e$ of more than 100%. However, the ion temperature fluctuations often exceed 100% and the measured fluctuations of $\bar{n}_e$ are less than 30%.[21]

Rugged magnetic fluctuation probes have been under development at the University of Wisconsin–Madison for many years.[22] The magnetic fluctuation measurements undertaken for these experiments have extended the frequency range of the previous fluctuation measurements in the MST from 1–250 kHz (Ref. 23) to 0.5–5.0 MHz. To improve the frequency response of the probe, a thin coating of a silver suspension was used as an electrostatic shield, instead of the normal stainless steel sheath. A detailed discussion of the response of small coils to short wavelength, high-frequency fluctuations is given in Ref. 22. All of the high-frequency fluctuation measurements were made at the plasma edge.

A compilation of the typical plasma parameters obtained during these experiments is given in Table I.

III. EQUILIBRIUM MEASUREMENTS

To fully investigate the temporal evolution of plasma parameters relevant to the study of ion heating in the RFP, a series of 200 identical RFP discharges were obtained. The equilibrium, shot averaged, charge exchange ion temperature for nearly one hundred 360 kA discharges is shown in Fig. 4. Relevant operational parameters are also shown in Fig. 4. They are: plasma current, loop voltage, and reversal parameter (F). Poor signal levels do not permit reliable charge exchange ion temperature measurements prior to $t=5$ msec; however, by $t=5$ msec, the ion temperature is already 150 eV. As can be seen from Fig. 4, the toroidal magnetic field does not reverse until $t=5$ msec. Thus, the rapid and intense ion heating occurs in the strongly relaxing, ultra-low-q magnetic configuration that occurs before the magnetic field at the edge reverses direction, i.e., before the plasma becomes a RFP. This configuration is quite similar to some of those early toroidal confinement experiments that exhibited anomalous ion heating.[7]

The Doppler broadened Cv 227.1 nm line was used to determine the impurity ion temperature. The ensemble averaged Doppler ion temperature and charge exchange ion

Downloaded 07 Jun 2006 to 128.104.165.52. Redistribution subject to AIP license or copyright, see http://pop.aip.org/pop/copyright.jsp

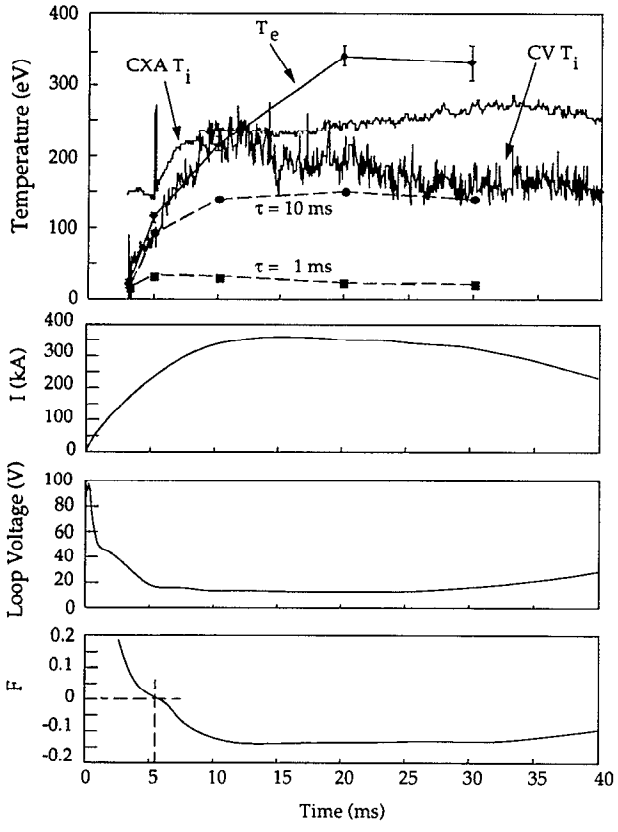

FIG. 4. Ensemble-averaged temperature and operational parameters for 99 identical discharges. Note that reversal occurs just after 5 msec. Top panel includes the average charge exchange (CXA) ion temperature, Doppler Cv ion temperature, Thomson scattering electron temperature, and the expected ion temperature due to electron–ion equilibration for two different ion energy confinement times (dashed lines).

temperature are also shown in Fig. 4. A typical fit to the Doppler measurements is shown in Fig. 3. The agreement, both in magnitude and early time evolution with the charge exchange ion temperature is evident. However, as the discharge current begins to decay, the charge exchange ion temperature increases, the Doppler ion temperature decreases, and the central electron temperature increases (Fig. 4). The ion temperature calculated from Cv emission reflects the local ion temperature, but the spatial distribution of C^{4+} ions is governed by the electron temperature magnitude and profile. Results from simulations using the MIST[24] code for MST parameters indicates that as the central electron temperature rises from 200 to 300 eV, the C^{4+} emission profile becomes hollow (Fig. 5). Therefore, as the electron temperature increases, changes in the Cv ion temperature simply reflect the character of the ion temperature profile as the location of the Cv emission varies.

The electron temperature is clearly lower than the ion temperature before 10 msec and then rises above the ion temperature (Fig. 4). This is a clear indication that the initial ion heating in the RFP cannot be explained by collisional transfer of energy from the electrons. To determine the energy balance within the RFP, the various densities are required. The central electron density was obtained from Thomson scattering, and the central neutral density

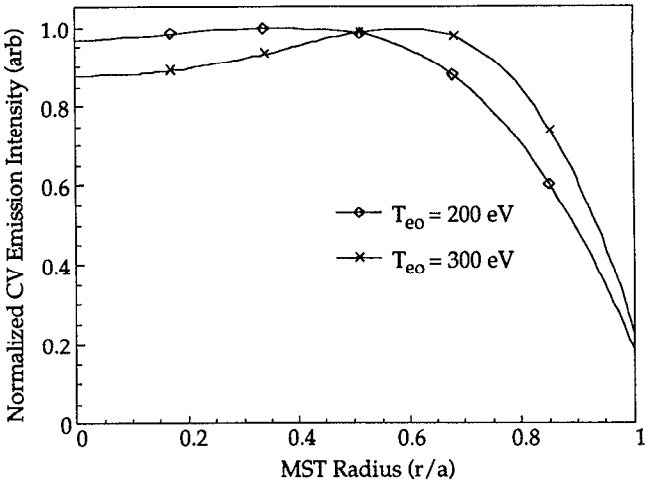

FIG. 5. Theoretical Cv (C^{4+}) distribution in the MST for two different central electron temperatures. Model uses a parabolic electron density and temperature profile, a particle confinement time of 1 msec, and $n_{e0}=1.0\times10^{13}$ cm^{-3}.

from the absolutely calibrated charge exchange analyzer. The absolute value of the calculated neutral density depends not only on the value used for the ion density (obtained from the electron density assuming $Z_{\text{eff}}=1$), but also on the profile and neutral transport assumptions discussed in the apparatus section of this paper. Previous calculations using H_α emission measurements and one-dimensional transport modeling yield a central neutral density of approximately 1×10^9 cm^{-3} in the MST, in good agreement with these results (Fig. 6).

To ascertain the significance of charge exchange power loss, the neutral flux over the energy range 93–2371 eV was measured (the nitrogen stripping cross section for hydrogen limits the lowest usable energy to approximately 100 eV). The neutral flux energy spectrum at 20 msec into the discharges is displayed in Fig. 7. An absolute conversion of the near-field, collimated neutral emission measured by the charge exchange analyzer into the total charge exchange power loss of the plasma requires complete density and temperature profile information and a full three-

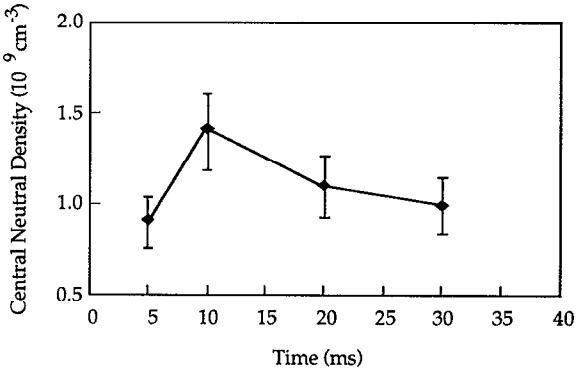

FIG. 6. Ensemble-averaged neutral density from the charge exchange analyzer.

Downloaded 07 Jun 2006 to 128.104.165.52. Redistribution subject to AIP license or copyright, see http://pop.aip.org/pop/copyright.jsp

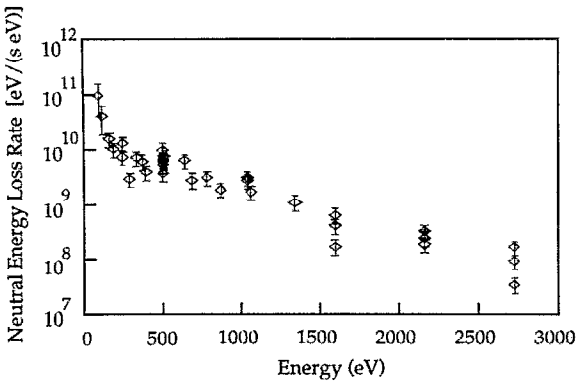

FIG. 7. Ensemble-averaged neutral flux spectrum 20.0 msec into the discharges.

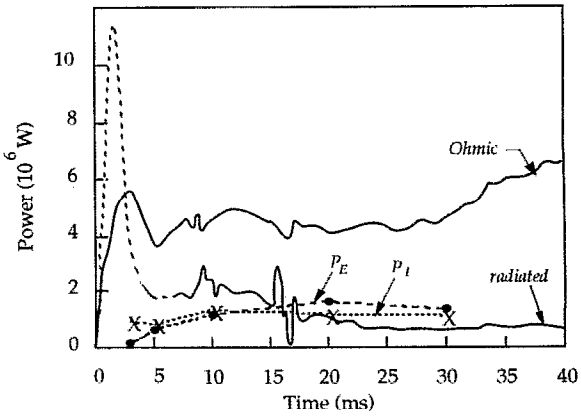

FIG. 8. Ensemble-averaged Ohmic power, radiated power, electron heating power (solid circles), and ion heating power (crosses).

dimensional calculation of the attenuation of neutrals born inside the plasma. Even if the theoretical profiles are used, the attenuation calculation is difficult. Neutrals that do not exit purely radially must be tracked laterally through the torus until they exit the plasma. With the added complication of multiple charge exchange collisions, keeping track of the neutral and ion densities along the trajectories of neutrals born everywhere within the plasma is beyond the scope of this paper.

Using the limiting case of an optically thin (no neutral attenuation) plasma, an upper bound for the total charge exchange power loss can be calculated from a single central chord measurement, $F(E)$. In the optically thin case, the neutral emission is nearly isotropic at the plasma surface. Thus, the charge exchange analyzer measures only a fraction of the neutral emission that passes through the collimation of the analyzer. Including corrections for the solid angles, collimation, and the unmeasured power below 100 eV (determined by NEUCG simulations) the total charge exchange power loss is less than 2% of the total input power, a negligible fraction.

Typically, the total power flowing into a plasma is obtained from measurements of the plasma current and the toroidal voltage. For MST, the measured toroidal voltage is converted into the Ohmic driving voltage using model profiles from the polynomial function model[25] (PFM) that account for the "twistedness" of the current path. The mutual inductance of the magnetic field circuits and the effects of the changing plasma current (dI/dt) are also taken into account. The product of the Ohmic driving voltage and the plasma current is the total input power and is displayed in Fig. 8 for the same discharges used in previous figures. The input power calculation is most reliable at peak current as dI/dt is zero. The radiated power for this set of discharges was measured with a bolometer and is also shown in Fig. 8. The bolometer is calibrated for a particular emission profile and the calibration is not valid during the formation phase of the discharge.[26]

Assuming an energy confinement time, τ_E, of 1 msec for the electrons and ions [a direct measurement of the ion energy confinement time will be presented in Sec. IV and previous electron energy confinement time measurements give $\tau_{Ee} \simeq 1$ msec (Ref. 17)], parabolic temperature and density profiles, and quasineutrality, the power required to maintain the measured equilibrium ion and electron temperatures can be estimated (Fig. 8). Figure 8 suggests that the power transported by the ions and electrons and emitted as radiation is sufficient to balance all of the power flowing into the plasma and serves as a crude check of the various temperature, density, and power loss measurements that have been presented.

The expected equilibrium central ion temperature due to ion–electron collisions (after the first 10 msec) is given by (all plasma parameters used are central values),

$$T_i = 7.5\times 10^{-8} \times \left(\frac{n_e}{\sqrt{T_e}[7.5\times 10^{-8}(n_e/T_e^{3/2}) + (3/2\tau_{Ei})]} \right), \tag{2}$$

where the ion–electron collision frequency is assumed to be of the form:[27]

$$\nu_E^{i/e} = \left(\frac{m_i}{m_e} \right) \left(\frac{4}{\sqrt{\pi}} \nu_0^{i/e} \right).$$

The ion temperatures obtained using (2) and the available electron temperatures and densities are shown in Fig. 4. Even an unreasonably large ion energy confinement time of 10 msec is insufficient to reproduce the measured ion temperatures late in the discharge.

The equilibrium ion temperature measurements unquestionably corroborate the noncollisional character of ion heating in the RFP as reported by other experiments.[3–6] It is possible that some noncollisional mechanism may exist that can transfer energy from the electrons to the ions in excess of collisional transfer rates. In order to generate ion temperatures greater than the bulk electron temperature, such a mechanism would have to preferentially transfer energy from the tail of the electron distribution to the ions. Experiments designed to examine

Downloaded 07 Jun 2006 to 128.104.165.52. Redistribution subject to AIP license or copyright, see http://pop.aip.org/pop/copyright.jsp

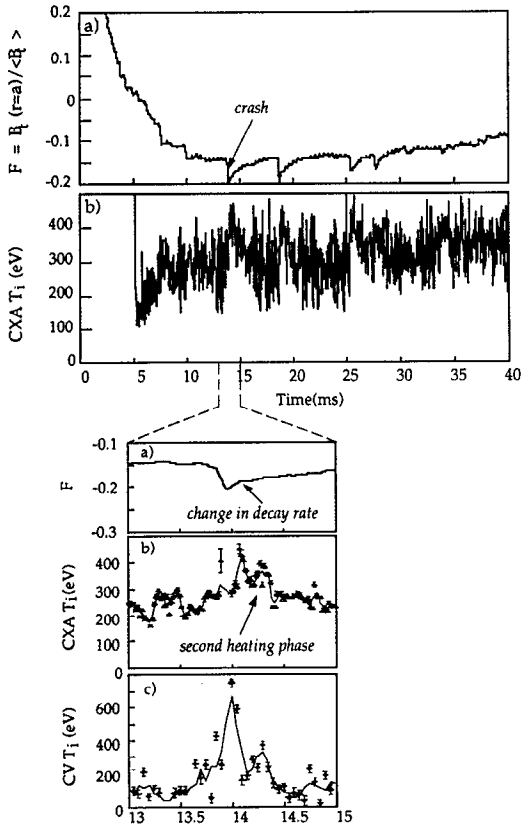

FIG. 9. Ion heating fluctuations are correlated with dynamo activity (a) reversal parameter (F), (b) charge exchange ion temperature, (c) Doppler ion temperature (there was not enough signal to the measure Doppler ion temperature throughout the discharge). Solid lines in (b) and (c) are the same data with three-point smoothing.

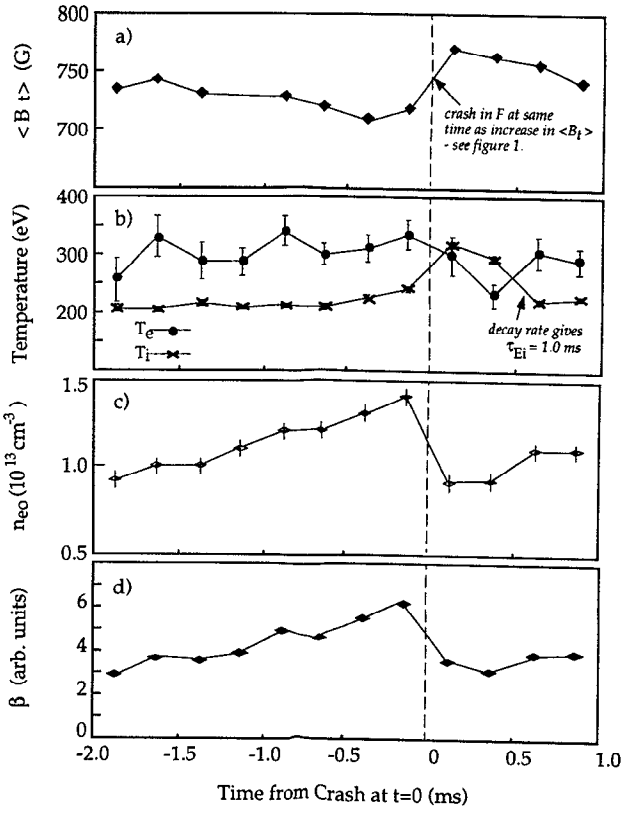

FIG. 10. Ensemble-averaged plasma parameters as a function of time from dynamo crash. (a) Average toroidal field, (b) central ion and electron temperature, (c) central electron density, (d) relative central β_0 versus time from dynamo burst crash.

the tail of the electron distribution in conjunction with ion heating are underway on the MST.

IV. NONEQUILIBRIUM ION TEMPERATURE MEASUREMENTS

During an individual discharge in the MST, sharp increases in the level of dynamo activity have been observed (Fig. 1). Coincident with each dynamo burst, the ion temperature is observed to increase sharply (Fig. 9). The correlation of the dynamo bursts and ion temperature increases appeared in every discharge examined. The expanded view of the dynamo burst at 14 msec of Fig. 9 includes Cv ion temperature results that were available because of higher Cv signal levels during the burst. The neutral energy spectrum often deviates from a simple Maxwellian during periods of rapid ion temperature change and a clearly non-Maxwellian energy spectrum is shown in Fig. 3. On both scales there is a clear correlation between the dynamo bursts and the onset of intense ion heating. In the expanded view, both ion temperatures even show the same sharp initial temperature rise just before 14 msec, a short cooling period, and a second increase in temperature as the decay rate of the dynamo burst suddenly slows around 14.25 msec. A possible explanation for the larger increase in the Cv ion temperature and the time delay between the Cv and the hydrogen heating (the Cv temperature rises first) will be proposed in Sec. V.

Using the crash phase of a dynamo burst as a reference, the single point electron temperature for a series of identical 360 kA discharges is plotted versus time from crash in Fig. 10(b). When multiple shots fell into the same time bin (when the Thomson scattering firing times were the same amount of time away from a dynamo crash), the raw Thomson scattering signals were averaged to generate a single electron temperature and density value. This analysis indicates that for these discharges, the electron temperature drops slightly just after a dynamo burst, and is relatively constant beforehand. The average toroidal field, also analyzed in the same manner as the Thomson scattering data, is shown in Fig. 10(a) to indicate the ensemble averaged, dynamo burst amplitude versus time from crash.

The charge exchange ion temperatures were analyzed in the same fashion and are displayed in Fig. 10(b). The ion temperature not only increases by more than 50%, it exceeds the electron temperature after the crash of the dynamo burst. The phase and decay rate of the ion temperature relative to the dynamo activity in the toroidal magnetic field is the same as for the single shot data (Fig. 9). The rise in the ion temperature is clearly correlated with the increase in toroidal magnetic field generation.

Downloaded 07 Jun 2006 to 128.104.165.52. Redistribution subject to AIP license or copyright, see http://pop.aip.org/pop/copyright.jsp

Assuming that no additional energy is flowing into the ions during the crash phase of the ion temperature, the ion energy confinement time can be obtained from the decay rate of the ion temperature. While the central electron density remains fairly constant [Fig. 10(c)], the ion temperature falls from approximately 300 to 200 eV in 0.5 msec. An exponential fit to the decay yields an ion energy confinement time, $\tau_{E\phi}$ of 1.0 msec.

The central density measured by Thomson scattering rises until the crash and then drops sharply [Fig. 10(c)]. In order to make a definitive statement about the density profile during dynamo bursts, experiments with simultaneous Thomson scattering and interferometer density measurements are underway. The central, relative plasma pressure $\beta_0 \propto n_0(T_{i0}+T_{e0})/B_0^2$, is also plotted versus time from crash in Fig. 10(d). Here, β_0 drops sharply, more than 50%, at the dynamo burst crash. It appears that energy confinement in the core decreases during the dynamo burst, even though the ion temperature increases.

These 10 μsec time-resolved ion temperature measurements confirm the hypothesis that dynamo fluctuations and ion heating are correlated in the RFP. The remaining, and perhaps most important, unanswered question concerning ion heating in RFP's is: what is the physical mechanism that transfers the energy from the external circuit to the ions? If the correlation between the increases in ion temperature and dynamo bursts is assumed to be causal; i.e., the correlation is due to the fact that energy flows from the fluctuations to the ions, the flow of energy out of the fluctuations should be detectable.

V. DYNAMO FLUCTUATION MEASUREMENTS

As it seemed likely that any number of instabilities could be enhanced during intense dynamo activity, the magnetic fluctuations in the MST were examined over as wide a frequency range as possible. The expectation was that the correlation of a particular instability with ion heating might be determined by studying the magnetic fluctuation power at the instability's characteristic frequency during the dynamo bursts. The first measurements were carried out in the frequency range 0.1–10 GHz. This range includes the electron cyclotron, electron plasma, and ion plasma frequencies for typical MST discharges. The very high-frequency (1–10 GHz) magnetic fluctuations were measured with an antenna inserted into the plasma edge. No measurable emissions were observed in this frequency range.

The low-frequency, 1–250 kHz, magnetic fluctuations have been examined in considerable detail.[23] Their mode structure suggests that they are dominated by tearing instabilities of frequency 10–30 kHz.[23] Tearing mode fluctuations are not expected to directly transfer significant amounts of energy to ions, but they are a source of free energy that can drive other instabilities or wave-particle resonances.[28] When the magnetic fluctuations in the frequency range 0.5–5.0 MHz were examined with the apparatus described earlier, a clear correlation of fluctuation amplitude with the dynamo bursts was observed (Fig. 11). The fluctuation level begins to rise well before the toroidal

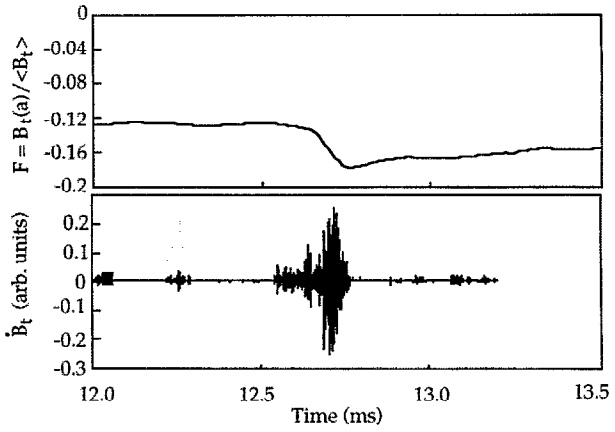

FIG. 11. Magnetic fluctuations (0.5–5.0 MHz) during a dynamo burst.

field is generated. After the fluctuation level plummets, the toroidal field begins to decay.

The power spectrum of the 0.5–5.0 MHz magnetic fluctuations was calculated for data records of either 12.8 or 25.6 μsec, 128 and 256 points respectively. Each record was preprocessed with a windowing function, usually a Hanning[29] window, to minimize finite record length effects. The built-in discrete fast Fourier transform function of the Interactive Data Language (IDL)[30] was used to generate the power spectrum. Rather remarkable structures often appear in the power spectra of individual time records. Two of the more dramatic examples are shown in Fig. 12; both use the same record length.

Dynamo bursts typically last 1 msec and the accompanying high-frequency fluctuations last approximately 0.25 msec. Using 12.8 μsec data records to obtain the best time resolution, the evolution of the power spectrum was examined for over 100 unsaturated dynamo bursts. A single dynamo burst and the corresponding change in ion

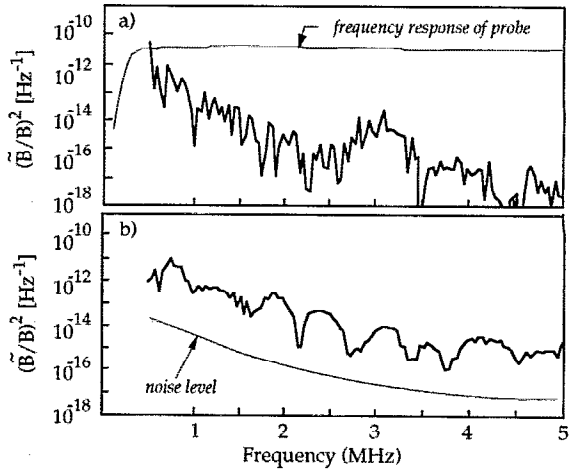

FIG. 12. Sample power spectrum features seen in 0.5–5.0 MHz magnetic fluctuations. The probe response on a log scale is shown in (a) and the dotted line in (b) is the measured noise level.

Downloaded 07 Jun 2006 to 128.104.165.52. Redistribution subject to AIP license or copyright, see http://pop.aip.org/pop/copyright.jsp

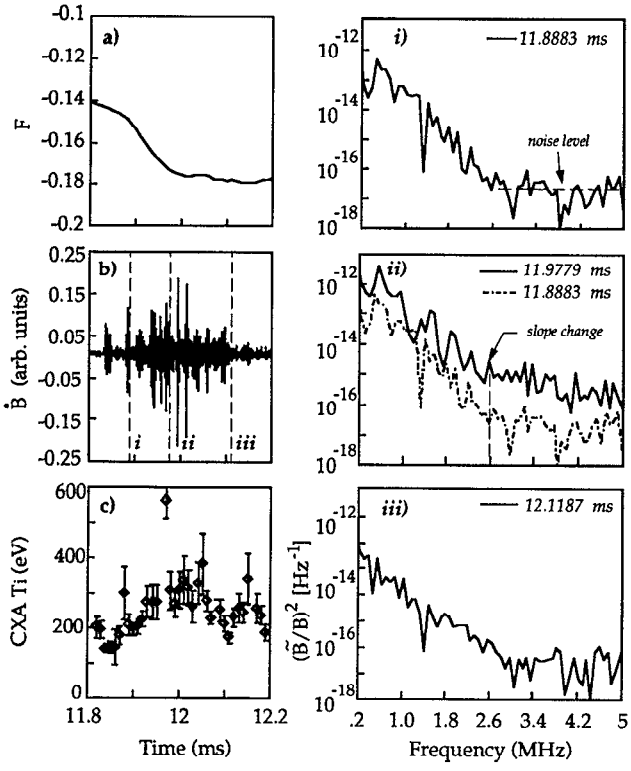

FIG. 13. Correlation of ion heating, high-frequency magnetic fluctuations, and power spectrum features: (a) Reversal parameter F during a dynamo burst, (b) high-frequency magnetic fluctuations, and (c) charge exchange ion temperature during the same burst. (i)–(iii) Frequency spectrum of the high-frequency magnetic fluctuations before, during, and after the dynamo burst. Change in slope feature indicated in frame (ii).

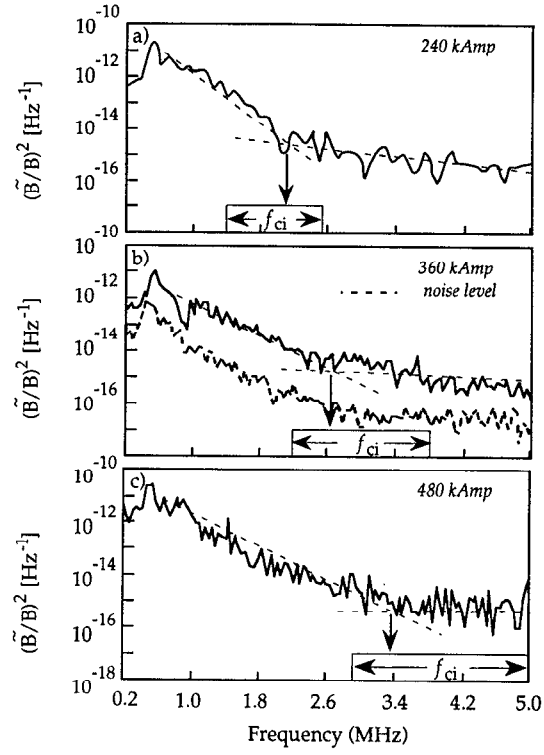

FIG. 14. Ensemble averaged frequency spectrum with dissipation feature for (a) 240 kA discharges—128 point records, (b) 360 kA discharges—256 point records, and (c) 450 kA discharge—256 point records. Location of the slope change feature determined from the second derivative of the data after five-point smoothing.

temperature for a 360 kA discharge is shown in Fig. 13, along with the power spectra for the times indicated.

Note that the slope of the power spectrum in Fig. 13(ii) changes at approximately 2.6 MHz. This feature is often, but not always, seen in the data record analyzed near the peak of the ion temperature. Why this feature is not seen every time is unclear. It is usually seen in the largest amplitude fluctuation measurements. Unfortunately, the majority of the largest amplitude high-frequency bursts saturate the digitizer and cannot be studied. It may be that only the strongest bursts retain information about core activity by the time they reach the MST edge. The weaker bursts may have their high frequency structure "washed out" before reaching the edge. The experimental results indicate that the weaker bursts have disproportionately smaller very high-frequency components than the larger amplitude bursts.

The relationship between fluctuations in the edge of the RFP and activity in the core is not well understood. There is no *a priori* justification for comparing the spectral evolution of edge magnetic fluctuations to central ion temperatures. The clear correlation of the high-frequency edge magnetic field bursts with the central ion temperature bursts is the only experimental evidence that links core and edge activity in the RFP.

Of the many characteristic frequencies possible for MST parameters, only the ion cyclotron frequency occurs near 2.5 MHz. To investigate whether the frequency spectrum feature is an ion cyclotron feature, the fluctuations were measured while varying the plasma current and similar bursts ensemble averaged. The results of the analysis are displayed in Fig. 14. The variation of ion cyclotron frequency with radius is indicated by the f_{ci} labeled regions in each panel of Fig. 14. The current scan results indicate a clear dependence of the frequency at which the power spectrum slope changes on the plasma current, i.e., the magnetic field (Fig. 15). This analysis strongly supports the hypothesis that the slope change frequency is an ion cyclotron feature.

A recent theoretical investigation by Mattor *et al.* into ion heating in the RFP has concluded that ion cyclotron resonances are the dominant mechanism for energy transfer to ions from small scale magnetic field fluctuations.[28] Their study divides the energy flowing into an RFP plasma between the fraction required to sustain the equilibrium fields and currents and the fraction stored in the MHD dynamo. Assuming that the dynamo is driven by the nonlinear coupling of tearing fluctuations,[23] the energy stored in the fluctuations is shown to cascade to smaller and smaller scales. Various dissipative effects and the scales at

Downloaded 07 Jun 2006 to 128.104.165.52. Redistribution subject to AIP license or copyright, see http://pop.aip.org/pop/copyright.jsp

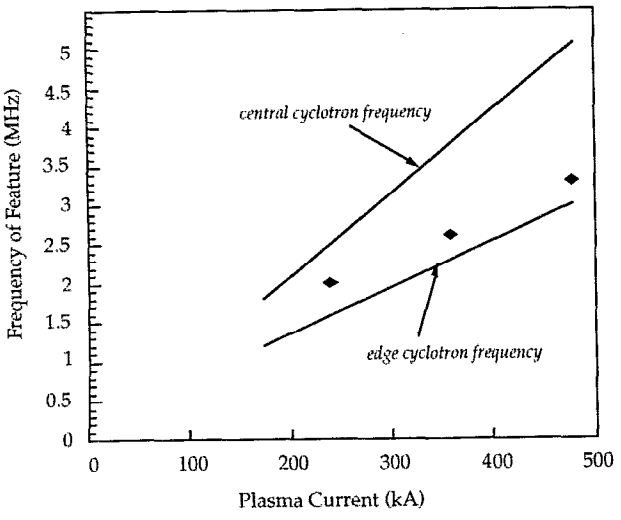

FIG. 15. Frequency of slope change power spectrum feature versus plasma current (diamonds). The solid lines are the cyclotron frequencies calculated for the total magnetic field. The slope change feature scales with current like the edge cyclotron frequency, but with an offset of approximately 0.7 MHz.

which they occur are examined and ion cyclotron resonance (ICR) dissipation is shown to occur at the largest scale. Other ion heating studies have suggested viscous dissipation as the most promising dissipative mechanism,[10,11] however, Mattor *et al.* show that, when calculated self-consistently, viscous effects occur at much smaller scales than ICR dissipation. The observed change in the frequency as a function of magnetic field at which energy is lost by the fluctuations (Fig. 14) does not support a viscosity based ion heating mechanism. However, the fact that the change in frequency tracks the ion cyclotron frequency strongly supports the ICR hypothesis.

ICR dissipation is a rapid energy transfer mechanism and the frequency, and therefore scale, at which the energy transfer occurs is mass dependent. As the fluctuation energy cascades to smaller and smaller scales, heavier mass ions will receive energy from the fluctuations before lighter ions as their ICR scale is larger. This may explain both the time lag and difference in magnitude seen in the CV and charge exchange ion temperatures (Fig. 9). Some of the very early ion heating studies in RFP's also suggested ion cyclotron effects as an explanation for anomalous ion heating in RFP's.[3]

A quantitative comparison with the Mattor–Prager–Terry model in the limit that all of the fluctuation energy goes into ion heating can be made during the dynamo bursts. During the dynamo bursts, the plasma current is fairly constant and the driving voltage increases substantially. If all of the additional input energy ($V_L I_p$) represents the increased fluctuation energy, and the fluctuation energy is used for ion heating in accordance with the Mattor–Prager–Terry model, the expected ion temperature change for the ensemble averaged dynamo burst of Fig. 10 is given by (assuming the transfer time is much faster than the ion energy confinement time, ≈ 1 msec):

$$\int_0^{\Delta t} I V_L^{\text{anom}}\, dt = \Delta \int \frac{3}{2} n_i T_i\, dV,$$

$$\int_0^{\Delta t} I V_L^{\text{anom}}\, dt = \frac{3}{2} \Delta (n_{i0} T_{i0}) V f,$$

where V is the volume of the MST, f accounts for the integral over the assumed density and temperature profiles ($f=1$ if both profiles are flat and $f=1/3$ if both profiles are parabolic), and V_L^{anom} is nonequilibrium component of the driving voltage. Solving for the stored ion energy change,

$$\Delta (n_{i0} T_{i0}) = \frac{\frac{2}{3}\int_0^{\Delta t} I V_L^{\text{anom}}\, dt}{Vf}, \tag{3}$$

using the Thomson scattering measured central electron density, and assuming $Z_{\text{eff}}=1$, the expected ion temperature at the peak of the ensemble-averaged dynamo burst of Fig. 10 is given by

$$(T_{i0})_{\text{peak}} = 260 \text{ eV} + 43 \text{ eV}/f.$$

The peak ion temperature in Fig. 10 is 320 eV, corresponding to a very reasonable profile factor of $f=0.7$. As this calculation assumed that all of the excess energy goes into ion heating, it is likely that the true profiles are more peaked than $f=0.7$ implies. If some of the excess energy does not end up in the ions, a smaller f (a more peaked profile) would be required to match the calculations of this model with the measured ion temperatures.

VI. DISCUSSION

No longer must a correlation between dynamo activity and high ion temperatures in the RFP be assumed. Our results provide substantial evidence that these two characteristics of the reversed field pinch are closely coupled. The equilibrium ion temperature has been shown to be unexplainable by simple ion–electron collisional heating. The nonequilibrium, dynamo burst, ion and electron temperatures confirm the lack of collisional coupling between the ions and electrons in the RFP. The correlation of the ion temperature and dynamo fluctuations suggests that a fluctuation dissipation mechanism is responsible for the bulk of the ion heating in the RFP and the frequency spectrum of the high-frequency magnetic fluctuations suggests enhanced energy dissipation near the ion cyclotron frequency.

Further measurements of the total energy budget of the RFP are needed for an effective and complete examination of anomalous ion heating in the RFP. These measurements will have to include full profile measurements of the temperatures, densities, and fluctuations in the RFP. Having seen the energy transfer effects of fluctuations in this work, and noting the on-going discussions of the strongly non-Spitzer character of the RFP plasma resistivity, we encourage the theoretical community to include fluctuations and major dissipative mechanisms in calculations of RFP plasma resistivities for inclusion in RFP energy budgets.

Downloaded 07 Jun 2006 to 128.104.165.52. Redistribution subject to AIP license or copyright, see http://pop.aip.org/pop/copyright.jsp

ACKNOWLEDGMENTS

We would like to thank Mike Cudzinovic, Curt Edmonds, Jerry Frank, Ed Haines, Paul Islye, John Laufenberg, Tom Lovell, and Nathan Mattor for their guidance and technical support during these experiments.

This work was supported by the U.S. Department of Energy, the Magnetic Fusion Science Fellowship program administered by Oak Ridge Associated Universities, and the Wisconsin Alumni Research Foundation.

[1]M. G. Rusbridge, Plasma Phys. **19**, 499 (1977).
[2]R. N. Dexter, D. W. Kerst, T. W. Lovell, S. C. Prager, and J. C. Sprott, Fusion Technol. **19**, 131 (1991).
[3]R. B. Howell and Y. Nagayama, Phys. Fluids **28**, 734 (1985).
[4]T. Fujita, K. Saito, J. Matusi, Y. Kamada, H. Morimoto, Z. Yoshida, and N. Inoue, Nucl. Fusion **31**, 3 (1991).
[5]G. A. Wurden, P. G. Weber, K. F. Schoenberg, A. E. Shofield, J. A. Phillips, C. P. Munson, G. Miller, J. C. Ingraham, R. B. Howell, J. N. Downing, R. R. Chrien, T. E. Cayton, L. C. Burkhardt, R. J. Bastasz, S. E. Walker, A. M. Prezler, P. G. Carolan, and C. A. Bunting, in *Proceedings of the 15th European Conference on Controlled Fusion and Plasma Physics,* Dubrovnik, Yugoslavia (European Physical Society, London, 1988), p. 533.
[6]P. G. Carolan, A. R. Field, A. Lazaros, M. G. Rusbridge, H. Y. W. Tsui, and M. V. Bevir, in *Proceedings of the 14th European Conference on Controlled Fusion and Plasma Physics,* Madrid, Spain (European Physical Society, London, 1987), Vol. II, p. 469.
[7]R. D. Bengtson, K. W. Gentle, J. Jancarik, S. S. Medley, P. Neilsen, and P. Phillips, Phys. Fluids **31**, 2266 (1988).
[8]T. M. Mayo and L. S. Kirschenbaum, Phys. Fluids B **3**, 2096 (1991).
[9]S. Hokin, A. Almagri, S. Assadi, J. Beckstead, G. Chartas, N. Crocker, M. Cudzinovic, D. Den Hartog, R. Dexter, D. Holly, S. Prager, T. Rempel, J. Sarff, E. Scime, W. Shen, C. Spragins, C. Sprott, G. Starr, M. Stoneking, and C. Watts, Phys. Fluids B **3**, 2241 (1991).
[10]C. G. Gimblett, Europhys. Lett. **11**, 541 (1990).
[11]Z. Yoshida, Nucl. Fusion **31**, 386 (1991).
[12]E. J. Caramana, R. A. Nebel, and D. D. Schnack, Phys. Fluids **26**, 1305 (1983).
[13]A. Fujisawa, H. Ji, K. Yamagishi, S. Shinohara, H. Toyama, and K. Miyamoto, Nucl. Fusion **31**, 1443 (1991).
[14]M. Giubbilei, P. Martin, and S. Ortolani, Plasma Phys. Controlled Fusion **32**, 405 (1990).
[15]E. Scime and S. Hokin, "Design and calibration of a fast-time resolution charge exchange analyzer," to appear in Rev. Sci. Instrum. (1992).
[16]E. Scime, Ph.D. thesis, University of Wisconsin—Madison, 1992.
[17]D. J. Den Hartog, Ph.D. thesis, University of Wisconsin—Madison, 1989.
[18]S. R. Burns, W. A. Peebles, D. Holly, and T. Lovell, "Madison Symmetric Torus far-infrared interferometer," to appear in Rev. Sci. Instrum. (1992).
[19]See, for example, I. H. Hutchinson, *Principles of Plasma Diagnostics* (Cambridge U. P., Cambridge, 1987).
[20]K. H. Burrell, J. Comput. Phys. **27**, 88 (1978).
[21]E. Scime, S. Hokin, N. Mattor, and C. Watts, Phys. Rev. Lett. **6**, 2165 (1992).
[22]E. Haines, Ph.D. thesis, University of Wisconsin—Madison, 1991.
[23]S. Assadi, S. C. Prager, and K. Sidikman, Phys. Rev. Lett. **69**, 281 (1992).
[24]R. A. Hulse, Nucl. Technol. Fusion **3** (1983).
[25]J. C. Sprott, Phys. Fluids **31**, 2266 (1988).
[26]M. Cudzinovik, Senior thesis, University of Wisconsin—Madison, 1991.
[27]D. L. Book, *NRL Plasma Formulary* (Naval Research Laboratory, Washington, DC, 1987), pp. 31–34.
[28]N. Mattor, S. C. Prager, and P. Terry, "Anomalous ion heating from the dynamo in a reversed field pinch," to appear in Comments Plasma Phys. Controlled Fusion. This work is also available from NTIS as Report No. DOE/ER/53212-177. Copies may be ordered from the National Technical Information Service, Springfield, VA 22161.
[29]W. H. Press, B. P. Flannery, S. A. Teukolsky, and W. T. Vetterling, *Numerical Recipes—The Art of Scientific Computing* (Cambridge U.P., New York, 1986), pp. 425.
[30]Interactive Data Language, Research Systems, Inc., 777 25th St. Suite 302, Boulder, CO 80303 (1988).

Downloaded 07 Jun 2006 to 128.104.165.52. Redistribution subject to AIP license or copyright, see http://pop.aip.org/pop/copyright.jsp